

The Effect of Pb Contamination on the Solidification Behavior of Sn-Bi Solders

Kil-Won Moon¹, William J. Boettinger¹, Ursula R. Kattner¹,
Carol A. Handwerker¹, and Doh-Jae Lee²

1- National Institute of Standards and Technology, Metallurgy Division,
100 Bureau Dr. Stop 8555, Gaithersburg, MD 20899-8555. 2- Chonnam National University,
Metallurgy Department, Kwanju, Korea 500-757

This paper presents experimental results and theoretical calculations to evaluate the effects of Pb contamination on the solidification behavior of Sn - x Bi alloys (x = 5, 10, and 58 mass %[†]). The pasty (mushy) range, the type of solidification path, and the fraction of the ternary eutectic are described. The experimental results are obtained from thermal analysis and quantitative metallography, and the solidification calculations are performed using Lever and Scheil assumptions. The experimental results agree with the Scheil calculations. The freezing range of Pb contaminated Sn-Bi solders is greatly increased due to the formation of a ternary eutectic reaction at (95.3 ± 0.5) °C. This increase is a likely cause of porosity in contaminated solder joints. The results provide an example of an analysis method for use in solder alloys in general.

Keywords: cooling curves, pasty range, Pb contamination, Sn-Bi solders, and Sn-Bi-Pb ternary eutectic

INTRODUCTION

Consideration of the harmful effects of Pb on the environment has prompted an effort to limit the use of Pb in manufactured products. In particular, the electronics industry is developing Pb-free alloys and adopting these alloys for commercial interconnect technologies.

Among the commercial Pb-free alloys, Sn-58 % Bi eutectic alloy may be a favorable alloy for consumer electronics and telecommunications.¹ In fact, this alloy, which has the eutectic temperature of 139 °C, has a higher ultimate tensile stress²⁻³ and shear strength²⁻⁴ than Sn-Pb eutectic. In addition, Sn-58 % Bi shows a slower creep rate and smaller rupture strain with small leading stresses than Sn-Pb eutectic.²⁻³ Although its fatigue life is shorter than Sn-Pb eutectic, the addition of 2 % Ag to Sn-58 % Bi improves its fatigue life dramatically.²⁻³

When Sn-Bi alloys are contaminated by Pb, which comes from the pre-tinned layer on components and pads,[‡] these alloys may form the ternary eutectic at 95 °C⁴ with a composition 51.5 % Bi-15.5 % Sn-33 % Pb.^{4,5} The low melting point of this ternary eutectic can degrade the mechanical properties of a solder joint. For example, Schmitt-Thomas and Wege⁶ showed that the fraction of porosity increases with thermal cycling in the temperature range of -40 °C to 100 °C because of melting of the Sn-Bi-Pb ternary eutectic. Strauss and Smernos⁷ reported that the shear strength and lifetime of Sn-Bi joints made on Cu pre-tinned with Sn-Pb eutectic

solder are worse than joints made on bare Cu.

However, the solidification behavior has not been quantitatively correlated to microstructures. Therefore, the purpose of this paper is to quantitatively evaluate the effects of Pb contamination on the solidification behavior by comparing experiments and theoretical calculations. First, the possible levels of Pb contamination in Sn-Bi solder joints are estimated, and the various possible types of solidification paths are calculated. The solidification path describes how the liquid concentration changes with temperature during solidification. It also describes the sequence and amounts of the various solid phases formed. With this information, three Sn-Bi alloys were chosen for the experiments, each with a different type of solidification path. Experimental cooling curves and metallography of these alloys are analyzed quantitatively and compared to the predictions of Lever and Scheil calculations. Also, possible effects of Pb contamination on the formation of porosity of Sn-Bi solder joints are discussed.

PROCEDURES

Lever and Scheil Calculations

The Lever or Scheil calculations are both based on the Sn-Bi-Pb equilibrium phase diagram. For the Lever calculation, complete mixing in the liquid and complete diffusion in

[†] In this paper, the percentage presents mass fraction, which is the same as weight fraction.

[‡] The changeover to Pb-free solder technology requires changes in pre-tinning operations as well as solder. As existing boards coated with Sn-Pb are used and as new tinning technologies are being developed, the possibility of Pb contamination exists.

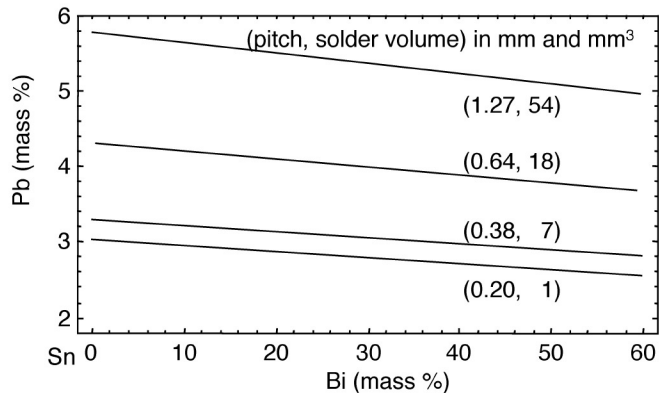


Figure 1. Calculated level of Pb contamination based on pitch, typical solder volume, and Sn-Bi composition for reflow process in surface mount technology. In this calculation, the pre-tinned thickness of 60 %Sn-40 %Pb solder was 7.5 μm .

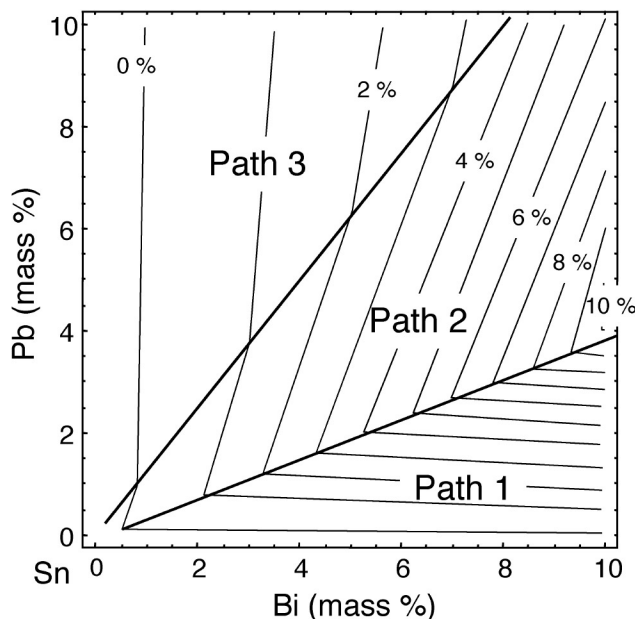


Figure 2. Lines of constant mass percentage of ternary eutectic and the three alloy composition regions with different types of solidification paths. Results are calculated using the Scheil assumptions.

the solid at each temperature are assumed, i.e., equilibrium solidification.⁸ For the Scheil calculation, complete mixing in the liquid but no diffusion in the solid at each temperature are assumed, i.e., considering only local equilibrium at the solid-liquid interface.⁸⁻⁹ The different assumptions of Lever and Scheil calculations give the minimum and maximum fractions of ternary eutectic that are possible. In the experiments, eutectic fractions must be intermediate between the predictions of the two calculations. Under most freezing conditions for substitutional solid solutions, such as those based on Sn,

the Scheil calculation is closer to reality. For example, the ternary eutectic structure will not appear during very slow equilibrium cooling for many alloys whereas the ternary eutectic will appear during normal cooling.

The maximum level of Pb contamination for a gull wing joint was estimated for four different pitches. The pitch is distance from center to center of adjacent pads. The typical solder volume used by industry for reflow process in surface mount technology depends on the pitch and is given in Figure 1. To compute the maximum level of Pb contamination, we assume that; 1) the contact area is the same on the pads and leads; 2) the contact area is a square with the side equal to one-half of the pitch; 3) the pads as well as the top and bottom of the leads are coated with 7.5 μm of 60 % Sn - 40 % Pb (we neglect the sides); and 4) complete dissolution of the pre-tinned layer occurs into the solder volume. The results are shown in Figure 1. A larger pitch and solder volume shows a higher level of the Pb contamination in a given Sn-Bi alloy. The maximum level of the Pb contamination is approximately 6 % Pb for a 1.27 mm pitch and 54 mm^3 typical solder volume.

To apply the Lever and Scheil calculations to the present research, thermodynamic parameters[†] for the phase diagram are obtained from Yoon and Lee,¹⁰ and the calculation method that is given by Boettinger et al.¹¹ is used. Scheil calculations are performed to estimate the fractions of the ternary eutectic for a range of Sn-Bi-Pb alloys with Pb contents between 0 % and 10 %. These results are presented in Figure 2. Also shown are three composition regions where the solidification path phase sequences are quite different. These are labeled Path I, II, and III, and the phase sequences are summarized in Table 1.

For all three predicted path types, the first (or primary) structure to solidify is the (Sn) phase. The secondary structure to solidify from the liquid at a lower temperature is a mixture of two solid phases (binary eutectic). For Path III, this secondary product of solidification changes to a different binary eutectic at a transition reaction: $L + (\text{Pb}) \rightarrow \text{Bi}_3\text{Pb}_7 + (\text{Sn})$.⁵ For all three paths, solidification is completed at the same final temperature (ternary eutectic temperature) by the solidification of three solid phases.

Materials

Sn-5 % Bi, Sn-10 % Bi and Sn-58 % Bi (the binary Sn-Bi eutectic is 57 % Bi) were chosen as representative of Sn-Bi binary solder compositions for the experiments. The Sn-Bi-Pb alloys were prepared from Sn-Bi alloy shot and Sn-Pb eutectic solder pellets by melting at 300 °C. When contaminated with 6 % Pb, the alloy compositions become Sn-4.2 % Bi-6 % Pb (Path III: Alloy C), Sn-8.4 % Bi-6 % Pb (Path II: Alloy B), and Sn-48.6 % Bi-6 % Pb (Path I: Alloy A), respectively. The compositions represent the three different types of predicted solidification path. In Table 2, the alloy compositions and the anticipated types of solidification path of the three alloys are listed.

[†] It should be noted that experimental data on the Sn-Bi-Pb eutectic in the literature⁵ gives two different temperatures, 100 °C and 96 °C for the ternary eutectic, Yoon and Lee¹⁰ selected the 100 °C temperature for their thermodynamic assessment. Therefore, the ternary eutectic temperature of Lever and Scheil calculations in this research is 100 °C. The present research supports the lower temperature.

Table 1. Types of Solidification Path from Scheil Calculations Noted in Figure 2

| | <i>Path I</i> | <i>Path II</i> | <i>Path III</i> |
|-----------|--|--|---|
| Primary | $L \rightarrow (\text{Sn})^\dagger$ | $L \rightarrow (\text{Sn})$ | $L \rightarrow (\text{Sn})$ |
| Secondary | $L \rightarrow (\text{Sn})+(\text{Bi})$ | $L \rightarrow (\text{Sn})+\text{Bi}_3\text{Pb}_7$ | $L \rightarrow (\text{Sn})+(\text{Pb})$ $L \rightarrow (\text{Sn})+\text{Bi}_3\text{Pb}_7$ |
| Tertiary | $L \rightarrow (\text{Sn})+(\text{Bi})+\text{Bi}_3\text{Pb}_7$ | $L \rightarrow (\text{Sn})+(\text{Bi})+\text{Bi}_3\text{Pb}_7$ | $L \rightarrow (\text{Sn})+(\text{Bi})+\text{Bi}_3\text{Pb}_7$ |

† The elemental symbol in parenthesis will be used to designate the solid solution phase based on this element in contrast to the pure component.

Table 2. Alloy Compositions

| <i>Uncontaminated Sn-Bi binary alloy</i> | <i>Contaminated alloy studied</i> | <i>Type of the solidification path</i> | <i>Alloy name</i> |
|--|-----------------------------------|--|-------------------|
| Sn - 58 % Bi | Sn-48.6 % Bi-6 % Pb | I | A |
| Sn - 10 % Bi | Sn-8.4 % Bi-6 % Pb | II | B |
| Sn - 5 % Bi | Sn-4.2 % Bi-6 % Pb | III | C |

Apparatus for Cooling Curves

Figure 3 shows the apparatus used to measure the cooling curve. Individual 5.6 ± 0.05 g (standard deviation) samples were prepared for cooling curve measurements. Samples were held at 250 °C for 2 h in a stoppered glass test tube and agitated every 30 min to mix thoroughly. An Inconel[‡] sheathed 250 μm (diameter) type K thermocouple was placed at the middle of the molten metal, and the glass sample container was inserted into a preheated (220 °C) graphite holder. The assembly was placed on a room temperature aluminum block for natural cooling to 50 °C. The measured average cooling rate was 27 °C/min, and an identical procedure was employed for each sample. After measuring the cooling curves, the samples were sectioned longitudinally for quantitative metallography.

This apparatus is quite simple and efficient to measure the cooling curve for low melting temperature alloys, especially. For instance, any thermal resistance between the thermocouple and sample is small. A fine sheathed thermocouple has a fast response time because of less thermal mass. An Inconel sheath reduces chemical reactions between the sample and thermocouple at low temperature. The air gap between the graphite tube and the glass test tube maximizes the signals of sample temperature changes by isolating the sample from thermal mass effects of the graphite tube. Finally, the large sample mass of this experiment improves the measurement of sample temperature changes and reduces effects of oxidation of the sample surface and heat extraction by the thermocouple. Therefore, it was expected that small change of the

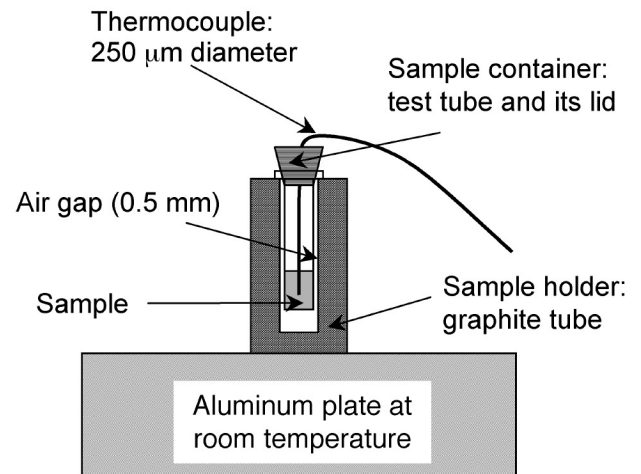


Figure 3. Schematic of the apparatus used to measure cooling curves.

sample temperature would be measurable during solidification.

Method to Analyze Solidification Behavior

An artificial cooling curve was constructed by first finding an exponential function that fit the measured cooling curve above the liquidus temperature. Due to release of the heat of fusion, the measured curve was shifted to later times compared to the exponential curve. The exponential curve was

‡ Trade names are used in this paper for completeness only, and their use does not constitute an endorsement by NIST.

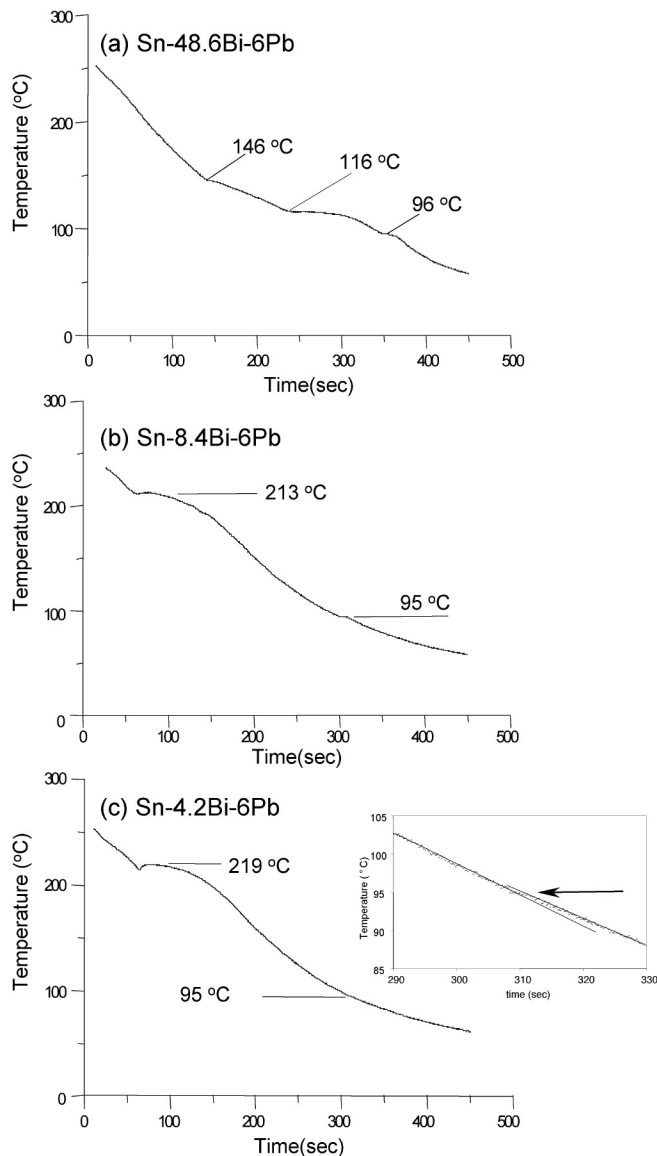


Figure 4. Measured cooling curves for the three alloy compositions. The detailed onset temperatures are indicated.

adjusted until the shapes of the measured and exponential curves matched below 70 °C. This procedure created a constructed curve that essentially had a constant time offset from the measured curve below 70 °C. We assumed that the constructed cooling curve represents the heat extraction of the sample without the evolution of the heat of fusion. The length of time spent on the ternary eutectic thermal arrest at 95 °C divided by the total offset time at, say, 50 °C gave a measure of fraction of the ternary eutectic. The temperature of 50 °C was chosen because the fit procedure was most accurate here.

From metallography, the type of the solidification path was obtained as well as the fraction of the ternary eutectic.

The mass fraction was determined by measuring the area fraction of the region of ternary eutectic microstructure from digitized pictures. The regions were identified by their characteristic microstructure (as described in the next section), manually outlined, and measured by a public domain software Image v1.62.[†] For accurate measurement, five pictures were analyzed, which covered about half of the sample cross section. In addition, the types of solidification path were determined from the microstructure. Finally, the Lever and Scheil calculations were performed for the three experimental compositions and compared to the experimental results.

RESULTS

The Pasty (Mushy) Range

The Pb contamination expands the temperature interval of the pasty range, which is the difference between the liquidus and final freezing temperature.[‡] From the cooling curves in Figure 4 and those conducted on uncontaminated Sn-Bi binary alloys, 6 % Pb contamination causes the measured pasty range of Sn-58 % Bi to change from 5 °C to 50 °C; Sn-10 % Bi, from 18 °C to 118 °C; and Sn-5 % Bi, from 14 °C to 124 °C. A large pasty range increases the tendency towards porosity and hot tearing due to the effect of alloy shrinkage and differential thermal contraction during solidification.¹² A large pasty range may also cause manufacturing problems, such as increasing the sensitivity to vibration during wave soldering.¹ In addition, this extensive pasty range may also increase the probability of fillet lifting phenomena in Dual-in-Line Package (DIP) through-hole joints.¹³ These freezing ranges are also larger than the 30 °C recommendation of NCMS.¹ Therefore, such Pb contamination is certainly undesirable.

Types of Solidification Path

To understand the various types of solidification path that were observed, the presence of different phases from metallography is considered along with the cooling curve events. In microstructures, the primary product of solidification is the coarsest and usually has a dendrite or grain like structure. The secondary and tertiary structures are successively finer. The identity of all phases was confirmed by energy dispersive X-ray analysis in a SEM.

For the microstructures of Sn-48.6 % Bi -6 % Pb shown in Figure 5-a and b, regions of primary (Sn) with (Bi) precipitates formed in the solid state, secondary Sn-Bi eutectic structure ((Sn)+(Bi)), and Sn-Bi-Pb ternary eutectic structure ((Sn)+(Bi)+Bi₃Pb₇) are identified. The sequence of phases formed agrees with the Type I path predicted for this alloy. Figure 6 shows a high magnification Backscattered Electron Image (BEI) of a ternary eutectic region. This region has a very fine three-phase mixture of (Bi) ($\geq 1-3 \mu\text{m}$; gray) and (Sn) ($\geq 1 \mu\text{m}$; dark) in a Bi₃Pb₇ matrix (the brightest area).

[†] This is contributed by NIH (URL: <http://rsb.info.nih.gov/nih-image/index.html>).

[‡] Under normal solidification conditions, the final freezing temperature is not the phase diagram solidus.

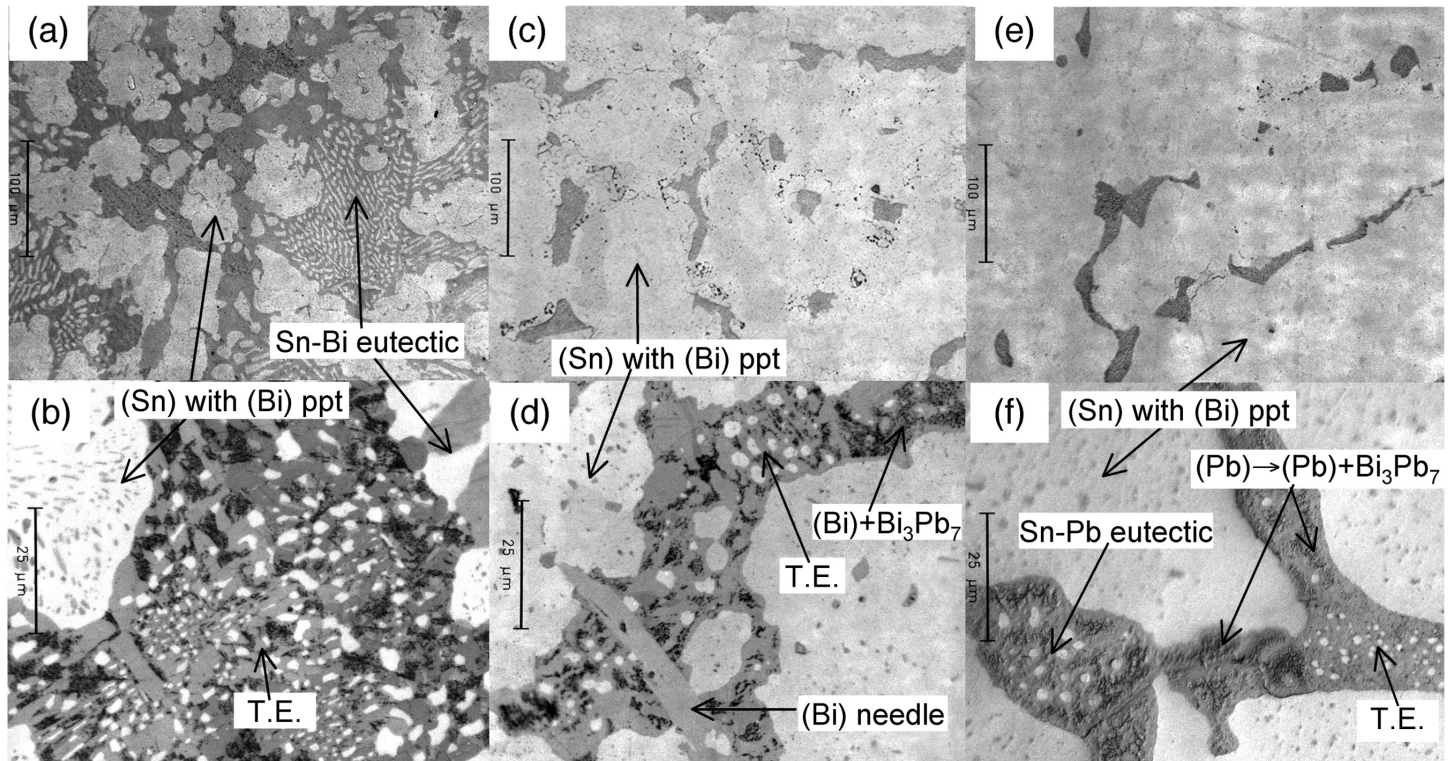


Figure 5. Optical microstructures observed after measuring cooling curves (a) and (b): Sn-48.6 % Bi-6 % Pb: alloy A; (c) and (d): Sn-8.4 % Bi-6 % Pb: alloy B; and (e) and (f): Sn-4.2 % Bi-6 % Pb: alloy C. Top three microstructures are at low magnification for a general view, and the bottom three microstructures focus on a ternary eutectic area (T.E.).

The ternary eutectic regions also contain micro-pores (circular $\leq 0.2 \mu\text{m}$) that are present only in the ternary eutectic ((Sn)+(Bi)+ Bi_3Pb_7) region. Thus, the presence of the micro-pores is used to identify the areas of the ternary eutectic for the quantitative metallography for the all alloys.

For Sn-8.4 % Bi -6 % Pb, Figure 5-c and d, primary (Sn) and Sn-Bi-Pb ternary eutectic ((Sn)+(Bi)+ Bi_3Pb_7) are present. The secondary (Sn)+ Bi_3Pb_7 eutectic structure is not present even though it was expected for the Type II path. The secondary structure is composed of a complex mixture of (Sn) particles, (Bi) needles and Bi_3Pb_7 +(Bi) regions. The complexity may be associated with a nucleation problem of the Bi_3Pb_7 phase. In this case, for example, Sn-Pb eutectic ((Sn)+(Pb)) and Sn-Bi eutectic structures ((Sn)+(Bi)) would be present instead of the (Sn)+ Bi_3Pb_7 eutectic structure. Furthermore, if the Sn-Pb eutectic structure is present, the transient reaction of $L + (\text{Pb}) \rightarrow \text{Bi}_3\text{Pb}_7 + (\text{Sn})$ should occur to reach the equilibrium. To understand this complexity, therefore, the study of a directional solidification, in addition to the thermal analysis from the present study, would be required. Nevertheless, the ternary eutectic structure is similar to Fig. 6.

In Figure 5-e and f, for Alloy C (Sn-4.2 % Bi-6 % Pb), the observed regions are primary (Sn), secondary Sn-Pb binary eutectic ((Sn)+(Pb)), a (Pb)+ Bi_3Pb_7 mixed region, and ternary eutectic structure ((Sn)+(Bi)+ Bi_3Pb_7). No secondary (Sn)+ Bi_3Pb_7 binary eutectic structure was observed. Again, the ternary eutectic region was identified by the presence of the fine porosity. In the ternary eutectic structure, (Bi) phase was essentially absent, unlike alloys A and B. At equilibrium,

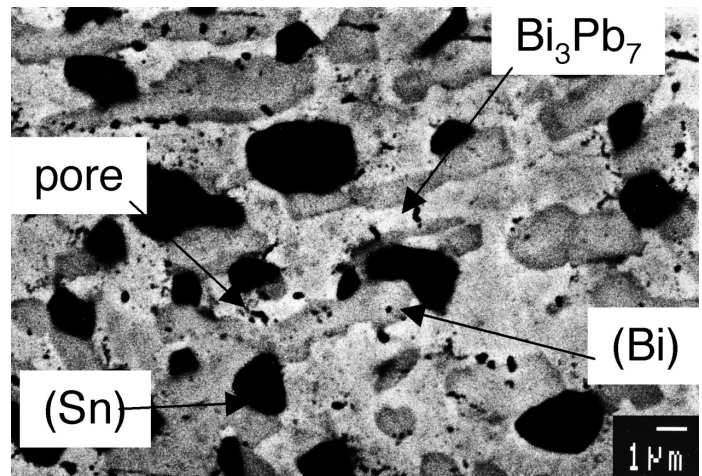


Figure 6. A BEI photomicrograph of the ternary eutectic microstructure in Sn-48.6 % Bi-6 % Pb: (Bi) ($\geq 1-3 \mu\text{m}$; gray), (Sn) ($\geq 1 \mu\text{m}$; dark), and micro-pores (circular $\leq 0.2 \mu\text{m}$) in a Bi_3Pb_7 matrix (the brightest area). The observed micro-pores are present only at this ternary eutectic region.

Alloy C should be composed only of (Sn) phase and Bi_3Pb_7 . Thus, there is a tendency for the (Bi) phase to dissolve due to solid state diffusion during and after solidification. This is particularly true for Alloy C because only 0.4 % of the total microstructure is predicted to be (Bi) phase by the Scheil analysis. We believe that the (Pb)+ Bi_3Pb_7 mixed region resulted from this solid state dissolution of (Bi).

Table 3 – Summary of Experimental Results and Comparison to Calculations

| Composition | Fraction ternary eutectic | | | | Onset of transition (°C) | | | |
|--|---------------------------|---------------------|--------|-------|---|-----------------------------|--------------------------|------------------------------|
| | Cooling Curves | Micro-structure | Scheil | Lever | Predicted Structure | Cooling Curves | Scheil | Lever |
| Sn - 48.6 % Bi - 6% Pb (Alloy A & Path I) | 0.164 ± 0.032 | 0.169 ± 0.055 | 0.18 | 0.174 | (Sn) (Sn) + (Bi) Ternary | 146 116 96 | 150 129 100 | 150 129 100 |
| Sn - 8.4 % Bi - 6 % Pb (Alloy B & Path II) | 0.059 ± 0.011 | 0.057 ± 0.011 | 0.060 | 0 | (Sn) (Sn) + Bi ₃ Pb ₇ Ternary | 213 ----- 95 | 213 121 100 | 213 134 ----- |
| Sn - 4.2 % Bi - 6 % Pb (Alloy C & Path III) | 0.011 ± 0.005 | 0.011 ± 0.004 | 0.014 | 0 | (Sn) (Sn) + (Pb) (Sn) + Bi ₃ Pb ₇ Ternary | 219 ----- ----- 95 | 219 150 138 100 | 219 161 ----- ----- |

From the cooling curves in Figure 4, the onsets of the solidification for Sn-48.6 % Bi-6 % Pb are observed at 146 °C for the primary (Sn), at 116 °C for the secondary Sn-Bi binary eutectic, and at 96 °C for the ternary eutectic. Onsets for primary (Sn) and ternary eutectic reactions were observed for Sn-8.4 % Bi-6 % Pb (213 °C, 95 °C) and Sn-4.2 % Bi-6 % Pb (219 °C, 95 °C). However, the onsets of the secondary binary eutectics, (Sn)+ Bi₃Pb₇, (Sn)+(Pb), and (Sn)+ Bi₃Pb₇, in these alloys were not detected.

Fractions of the Ternary Eutectic

Fractions of the ternary eutectic are measured from the cooling curves and metallography as described in the paragraph on the analysis of the solidification behavior. From the cooling curves, the measured fraction for Alloy A is 0.164 ± 0.032 ; Alloy B, 0.059 ± 0.011 ; and Alloy C, 0.011 ± 0.005 . The uncertainties are estimated using different interpretations of the locations of slope changes on the cooling curves. From the micrographs, the measured fractions are 0.169 ± 0.055 for Alloy A, 0.057 ± 0.011 for Alloy B, and 0.011 ± 0.004 for Alloy C. The uncertainties are estimated using differences among the five micrographs taken for each sample.

DISCUSSION

Comparison of the Experimental Results to Calculations

Table 3 summarizes the experimental results and the Scheil and Lever calculations. The solidification paths are shown in Figure 7. The agreement between the metallographic results and the thermal results for the fraction of eutectic is excellent. As stated in the introduction, the experimental results should agree better with the Scheil calculations. The Lever calculations show the formation of the

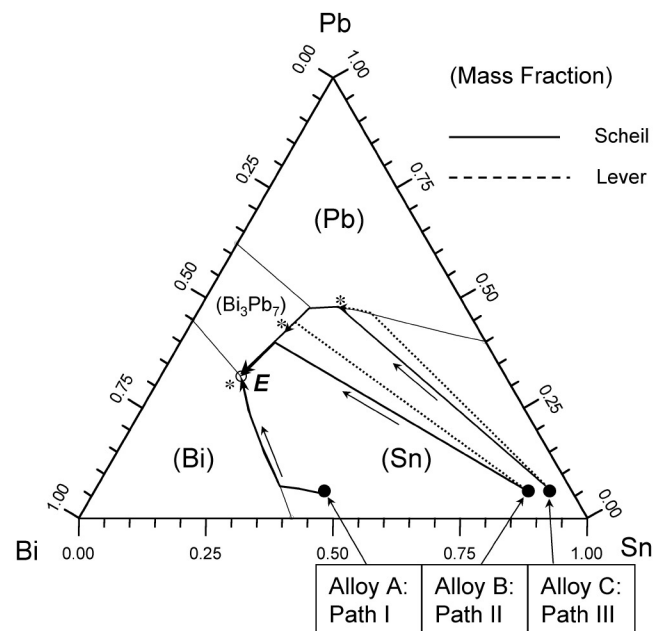


Figure 7. Calculated liquidus surfaces of Sn-Bi-Pb with superimposed solidification paths for the three alloys using Lever and Scheil calculations. For alloy A, the Scheil and Lever predictions are about identical. For alloy B and C, the star marks the compositions that are the final composition of the liquid from the Lever calculations. For the Scheil calculations, the final liquid composition is the ternary eutectic (point E).

ternary eutectic only for Sn-48.6 % Bi-6 % Pb. The difference between the Lever and Scheil calculations of Sn-8.4 % Bi-6 % Pb and Sn-4.2 % Bi-6 % Pb indicates that the ternary eutectic formed during solidification would disappear after sufficiently long annealing. The results of the Lever calculations of Sn-48.6 % Bi-6 % Pb are almost identical to the results of the Scheil calculations since this composition is

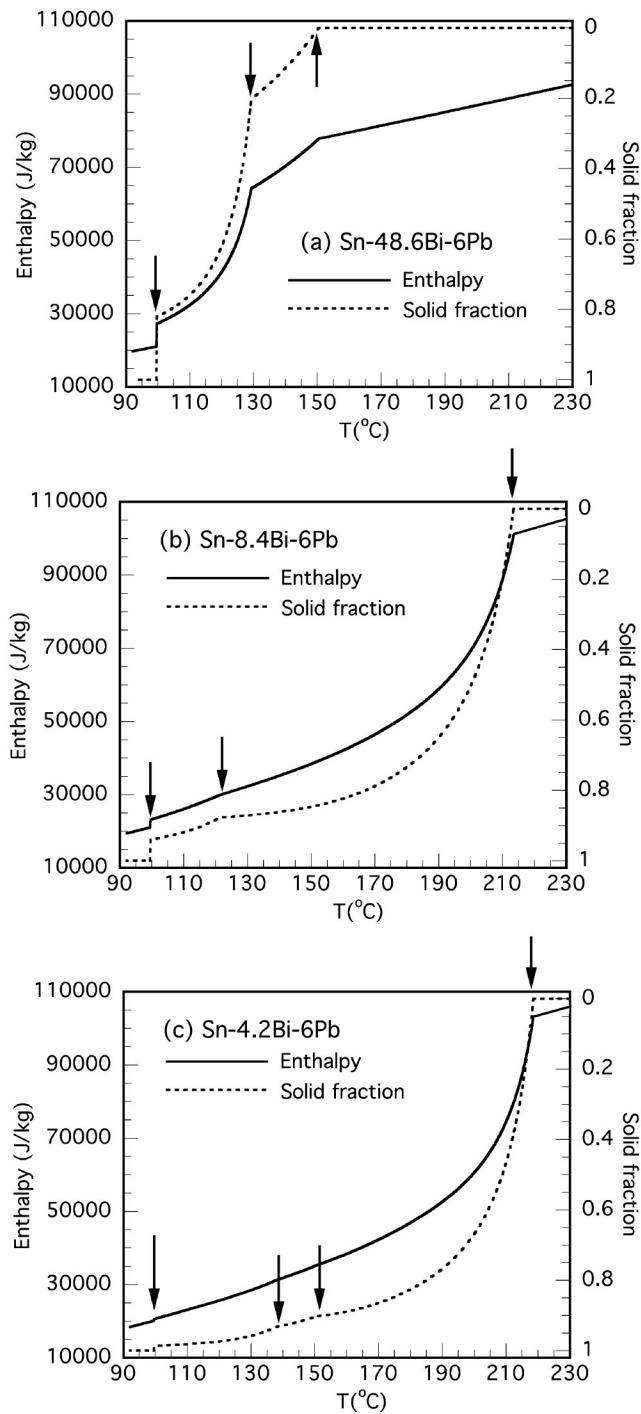


Figure 8. Calculated curves of enthalpy and solid fraction as a function of temperature using the Scheil assumption: (a) Sn-48.6 % Bi -6 % Pb: alloy A, (b) Sn-8.4 % Bi -6 % Pb: alloy B, and (c) Sn-4.2 % Bi-6 % Pb: alloy C. Arrows indicate the onsets of the stages of solidification.

near the Sn-57 % Bi binary eutectic composition and has very little primary (Sn) phase to permit segregation during solidification.

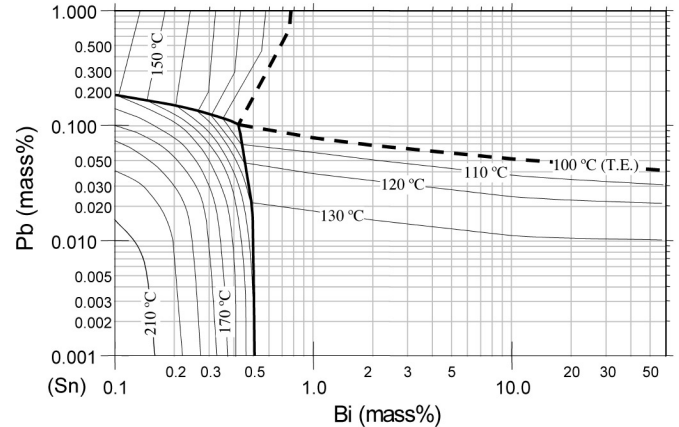


Figure 9. Calculated final freezing temperature using Scheil assumptions for alloys of the designated composition.

Several onset temperatures for the secondary solidification structures were not observed (Table 3). This may be due to the complex nature of these microstructure regions as shown in Figure 5-d and 5-f; e.g., nucleation problems associated with the phases in the various secondary binary eutectics. In addition, examination of the enthalpy-temperature curves, obtained from the Scheil calculation, is elucidating. Figure 8 presents the enthalpy H and the total solid fraction f_s as functions of the temperature T . The changes in enthalpy indicate the heat extraction associated with the formation of the solid structure. For each stage of solidification (primary, secondary, and tertiary), the onset temperatures in a cooling curve is indicated by a discontinuous change in slope. The size of the slope change in a cooling curve is proportional to the size of the slope change of the enthalpy vs. temperature curve corresponding to the beginning of that stage of solidification. The enthalpy change of Sn-48.6 % Bi-6 % Pb alloy has a large change of dH/dT for all three stages. The values of dH/dT for the secondary stage of solidification for Sn-8.4 % Bi-6 % Pb and Sn-4.2 % Bi-6 % Pb are very small. This is another reason why onset temperatures for these stages could not be easily measured experimentally. Equivalently, a very small change in df_s/dT corresponds to the beginning of secondary solidification in these cases.

Final Freezing Temperatures

Because of the good agreement between the measured and calculated fraction of the ternary eutectic, we have performed Scheil calculations giving the final freezing temperature for a range of alloys with very low (<1%) Pb contents. These results are shown in Figure 9. In the upper right region of Figure 9, with a final freezing temperature of 100 °C, the ternary eutectic forms as already noted in Figure 2. The 0.1 % Pb contamination promotes the formation of the ternary eutectic in Sn- x Bi ($x \geq 0.5$ %) alloys. For Sn-Bi solders with lower Pb (or Bi) contents, the final freezing temperature increases gradually from the ternary eutectic temperature as given in Figure 9. However, this increase is much lower than the increase of the final freezing temperature of Sn-Bi

binary alloys. In fact, 0.1 % Pb contamination reduces the final freezing temperature of Sn-Bi binary alloys by 38 °C to 55 °C depending on the Bi content. While the final freezing temperature decreases drastically, the liquidus temperature reduction for the same Pb contamination is only ~ 1 °C. As a result, the discrepancy introduces an expansion of the pasty range. Therefore, for reliable solder joints of Sn-Bi alloys, Pb contamination should be avoided to prevent the formation of the ternary eutectic and the increase of the pasty range.

Porosity

One of the critical problems for Sn-Bi solder due to Pb contamination is the formation of extensive porosity that can degrade mechanical properties of the solder joint, specifically in Leadless Ceramic Chip Carrier (LCCC) joints.⁷ Usually, the porosity in a LCCC joint after thermal fatigue tests is observed in the narrow gap between the component and the pad.¹ Due to the thermal mass of the component and the pad, the gap area cools more slowly than the bulk area of solder. This means that this region is the last to freeze, and porosity and/or hot tearing is most likely to form in this region during soldering. The hot tearing is amplified whenever the freezing range is enlarged. In addition, thermal cycling above the ternary eutectic temperature of 95 °C can cause an active flow of the molten solder and modification of the microstructure leading to premature failure.

SUMMARY

The effects of Pb contamination on the solidification behavior of Sn-x Bi (x = 5, 10, and 58 mass %) alloys have been investigated. Pb additions as small as 1% to Sn-Bi alloys, drastically expand the freezing range due to the formation of a ternary eutectic at 95.3 °C. The phase sequence formed during solidification agrees with Scheil calculations. The measured fractions of the ternary eutectic for Sn-Bi-Pb alloys obtained from thermal and metallographic analysis also agree with Scheil calculations. Finally, the possible formation of the extensive porosity is discussed; e.g., the localized ternary eutectic may increase the formation of the extensive porosity.

REFERENCES

1. Lead-Free Solder Project Final Report: NCMS Report 0401RE96 (Ann Arbor, MI: National Center for Manufacturing Sciences, Aug., 1997).
2. Fay Hua, Zequn Mei, and Judy Glazer, "Eutectic Sn-Bi as an Alternative to Pb-Free Solders," in Proc. of IEEE Electronic Components and Technology Conference, (1998) pp. 277-283.
3. J. Glazer, *Inter. Mater. Rev.*, Vol. 40, No. 2, (1995) pp. 65-93.
4. H. Schumann, Metallographie, (VEB Verlag, Leipzig, 1974) pp. 229-230.
5. P. Villars, A. Prince, and H. Okamoto (editor), Handbook of Ternary Alloy Phase Diagrams, Vol. 5, (Materials Park, OH: ASM International, 1995), pp. 6373-80.
6. Kh. G. Schmitt-Thomas and S. Wege, *Brazing and Soldering*, No.11, Autumn (1986) pp. 27-33.
7. R. Strauss and S. Smernos, *The Bulletin of the Bismuth Institute*, Vol. 49, (1986) pp. 1-4.
8. Merton C. Flemings, Solidification Processing, (New York: McGraw-Hill, 1974) pp. 33-36.
9. H. Biloni and W.J. Boettinger, "Solidification," Physical Metallurgy, ed. R.W. Chan and P. Haasen (New York: North-Holland, 1996) pp. 714-716.
10. S. W. Yoon and H. M. Lee, *Calphad*, Vol. 22, No. 2, (1998) pp. 167-178.
11. W.J. Boettinger, U.R. Kattner, S.R. Coriell, Y.A. Chang, and B.A. Mueller, "Development of Multicomponent Solidification Micromodels Using a Thermodynamic Phase Diagram Data Base," in "Model of Casting, Welding and Advanced Solidification Process VII," Eds. M. Cross and J. Campbell (TMS, Warrendale, PA, 1995) pp. 649-656.
12. W. Kurz and D.J. Fisher, Fundamentals of Solidification, (Switzerland: Trans Tech SA, 1984).
13. W.J. Boettinger, C.A. Handwerker, B. Newbery, and T.Y. Pan, "Observation of Fillet Lifting in Sn-Bi Alloys," Unpublished research.